applied sciences

MDPI

Article

Micromechanical Characterization of Diatom Frustules of Multiple Origin

Daniel Zuluaga-Astudillo [1,2,*], Juan Carlos Ruge [2,*] and Bernardo Caicedo-Hormaza [3]

[1] Programa de Diseño y Construcción de Vías y Aeropistas, Escuela de Ingenieros Militares, Ejército de Colombia, Bogotá 111611, Colombia
[2] Programa de Doctorado en Ingeniería, Universidad Militar Nueva Granada, Bogotá 110111, Colombia
[3] Departamento de Ingeniería Civil y Ambiental, Universidad de los Andes, Bogotá 110311, Colombia; bcaicedo@uniandes.edu.co
* Correspondence: daniel.zuluaga@esing.edu.co or est.daniel.zuluaga@unimilitar.edu.co (D.Z.-A.); juan.ruge@unimilitar.edu.co (J.C.R.)

Abstract: The siliceous structure that protects diatoms, called frustule, is the main component of diatom sedimentary soils. These particles' physical and mechanical characteristics are challenging, given their geometric conditions of only a few microns. For this evaluation, specialized tools must be used, such as the Scanning Electron Microscope (SEM), the Atomic Force Microscope (AFM) and X-ray dispersion (XRD), among others. The bibliographic references show significant variability in the "load-deformation" behavior in frustules, diatoms or their organic components. Technical background information usually presents information on a single type of species. This research demonstrated the characterization and micromechanical evaluation of frustules of three morphologically distinguishable species of diatoms (Colombian, Mexican and Peruvian origin). The results showed similarities in the chemical composition of the three samples. The displacement records are variable depending on the species for the same load range. The location of the load application points by AFM on the different types of frustules is presented. The most significant deformation in the Mexican species and the regularity in the results of the Peruvian species stand out. Young's moduli were also calculated by applying the Hertz Model, which had the highest values in the Colombian sample.

Keywords: diatomaceous soil; frustule; atomic force microscopy; force-displacement curves

check for updates

Academic Editor: Andrea Frazzica

Received: 20 October 2024
Revised: 17 December 2024
Accepted: 26 December 2024
Published: 14 January 2025

Citation: Zuluaga-Astudillo, D.; Ruge, J.C.; Caicedo-Hormaza, B. Micromechanical Characterization of Diatom Frustules of Multiple Origin. *Appl. Sci.* **2025**, *15*, 749. https://doi.org/10.3390/app15020749

Copyright: © 2025 by the authors. Licensee MDPI, Basel, Switzerland. This article is an open access article distributed under the terms and conditions of the Creative Commons Attribution (CC BY) license (https://creativecommons.org/licenses/by/4.0/).

1. Introduction

Diatoms are unicellular algae with a siliceous skeleton called a frustule [1,2], and they are present in almost all aquatic environments (fresh and salty) [3]. After their death and organic decomposition, the frustules are deposited at the bottom of water bodies, forming Diatomaceous Soils (DS) [4–6]. These fossils can be found whole or as fragments within the clay, organic, siltstone or quartz matrices [7]. Particles are characterized by having different pore patterns, shapes and sizes. These Silica structures are solid residues of metabolic processes [8,9]. Diatoms have not become extinct due to their frustules' protective action, which presents supernormal mechanical characteristics, such as a high elastic modulus, which gives them restorative properties when subjected to loads and deformations [10,11].

The surface properties of diatoms and their frustules should be analyzed at the macro scale, corresponding to the total shape of the shells, and at the nanoscale, related to pore networks and wall thickness. The frustules support external and internal mechanical loads due to predation, turgor and reproductive processes [9]. Sediments rich in diatoms present

different physical properties from those categorized as organic and inorganic. Conventional geotechnical methods cannot completely characterize it [12,13].

Scanning Electron Microscopy (SEM) is a small-scale visualization technique [14]. It provides information on the observed particles' topography, morphology, shape, size, composition and crystallographic structure [15,16]. The behavior of some soils (silts, clays, DS) is only sometimes understood from the results of physical and mechanical tests. In such cases, it is necessary to assess the microstructure and fabric through SEM. Traditional characterization and mechanical evaluation tests need to provide more information about DSs [17]. From SEM tests, it has been possible to conclude that Diatomaceous Soils are mostly pure biogenic opal, with some mechanical alteration or fragmentation level.

The quantity of fractured or intact diatoms inside another type of soil matrices depends on environmental factors [18]. This condition (breakup and rearrangement) of particles is corroborated through microscopy techniques [19].

Atomic Force Microscopy (AFM) allows for obtaining high-resolution 3D images from the change in surface height of the observed particle. It is applied to advanced studies of deformation, adhesion, Young's modulus, and nano and micromechanical properties, among others [20–22]. The AFM consists of a micromachined elastic cantilever with a sharp tip perpendicular to the cantilever. When a force is applied to the tip, the cantilever deflects. From AFM, stress and strain records can be obtained, even on the scale of single molecules [23]. About diatoms, AFM has been implemented for the total assessment of the cell through the progressive application of loads on its frustule, up to the point of reaching rupture, as well as for the evaluation of local properties, i.e., the strength of the different elements that make up the structure.

The—*Cs*—swelling index obtained in a one-dimensional consolidation test on diatomaceous soil is up to twice as high as those recorded for kaolin-type soil [24]. This phenomenon can be associated with the elastic properties of diatom frustules. Diatoms are not entirely rigid and show considerable elastic deformation before breaking [11]. Diatom-rich sediments can, therefore, "remember" the stress regime in situ. However, these soils are not cohesive and can quickly lose or acquire water, which generally disturbs the samples and leads to the loss of stress memory [24].

After reviewing state-of-the-art regarding the application of microscopy techniques in diatomaceous fossils, the present research aimed to physically, chemically and mechanically characterize, by SEM and AFM observation, diatom frustules of three morphologically distinguishable species (Peruvian, Mexican and Colombian origin). "force-displacement" records were obtained due to the application of loads at different points of the fossils. Likewise, it was possible to determine Young's moduli. The above is to comprehend the particles' mechanical behavior and differentiate their responses according to origin, composition and morphology.

2. State-of-the-Art

Diatoms are eukaryotic, photosynthetic, and unicellular. Its growth depends on physical and chemical surrounding conditions, particularly turbidity, temperature, pH, nutrients, and salinity. These algae develop a siliceous skeleton denominated "frustule" [1–3,9,25].

Their growth depends on the concentration of Vitamin B12, amount of light, dissolved silica, nitrogen and phosphorus, and they are considered indicators of water quality [26,27].

After the death and organic decomposition of the algae, the frustules are deposited on the bottom of oceans or lakes, forming Diatomaceous Soils [4–6]. These soils have been found in different parts of the world, such as the United States, China, Peru, Japan, Denmark, Mexico, Colombia, Argentina, polar and equatorial belts, and the South American subduction zone. Frustules can be found whole or as remains of opalized algal cells

incorporated within clay, organic, siltstone or quartz matrices [7]. The deposits result from the accumulation of amorphous silica from the frustules of diatoms [28].

Diatoms extract silica from their natural aqueous environment, forming the frustules. Silica can come from solutions in streams, by the reaction of adjacent rocks, or by the influx of volcanic ash. Phosphorus is the primary nutrient, mainly from the weathering of nearby rocks [29]. Diatoms play a significant global role in the biochemical cycling of carbon and silica in the water column [30]. Frustules are notable for having multiple pores or areoles, elongated, spherical or disk shapes, and variable sizes between 10 and 200 μm [8].

Diatom cells have two overlapping elements (thecas): the external (epitheca) and the internal (hypotheca). Their composition is about 95% polymerized silicic acid, similar to quartz. Two types of diatoms are recognized: pennate and centric. The first presents bilateral symmetry, which is usually found in freshwater. The second report is on radial symmetry, which is related to marine environments [13,31–33].

The fossil record indicates that they evolved from the Cretaceous; fossil diatom deposits from the end of this period are known as diatomaceous earth [26]. The "ornamentations" or characteristic descriptions of the frustules are caused by the differential arrangement or attachment of silica in the cell wall [26] and are helpful for visual classification [33].

2.1. Taphonomic Processes in Diatom Frustules

Taphonomy studies the transition "biosphere—lithosphere" in organic remains. These analyses start with an organism's death or the detachment of some of its parts. Taphonomy studies facilitate the interpretation of fossil records. Unlike organic remains, the number of living organisms preserved as fossils is minimal [34]. Diagenetic variations are technically defined as taphonomic processes. Some Japanese marine diatomaceous soils (micro remnants) present particles (plant and animal) usually less than 1 mm in size [13].

The formation of frustules occurs by the polymerization of silicic acid within the deposition vesicles (low pH environment) [2]; this process involves cell components such as the cytoskeleton, the mitochondria, the endoplasmic reticulum, the Golgi apparatus and the plasmalemma membrane [35]. Silica spheres conforming to diatom frustules are considered impermeable and solid excrement. The frustule's evolutionary adaptations have made it dominant in cell physiology and morphogenesis [9].

The extent of silicification of frustules depends on the rate of Silica fixation, either by the availability in the environment or by the effectiveness and genomic characteristics of its transporters [36,37], except for exceptional cases that do not require higher Silica content for cell development. Silica concentration defines frustules' growth; its presence generates ballast necessary in the sedimentation process. Silica concentrates mainly in the photic zone of aquatic environments [38].

Silica in aquatic environments is found mainly in the form of silicic acid $Si(OH)_4$. It is usually transformed into solid silicon oxide, SiO_2, or other siliceous compounds in the presence of organic substances by condensation processes [39] or by diffusion through the membranes of diatoms. When low silicic acid concentrations are in the aquatic environment, cells activate transporters that facilitate fixation [30,40]. Unlike nitrogen and phosphorus metabolization, silica uptake in diatoms mainly relates to aerobic respiration processes and not so much to photosynthetic processes [30,41].

The acid accumulates temporarily in the deposition vesicles. Then, by the interaction of specific proteins, polyamines and elements of the cytoskeleton, the amorphous Silica is deposited in the form of small spheres, together with some organic matter (organic components can lead to the formation of bacteria, which retard cell growth [30]), in the strict ordering patterns presented by the frustules. This process involves a relatively low energy expenditure (2% of the diatom's energy reserves due to a frustule with 25%

silica). It is primarily concentrated in the stage of silicic acid transport across the plasma membrane [2]. Frustules are multilayered porous structures with remarkable mechanical properties (Elastic Modulus 22.4 GPa) and restorative properties when imposed loads and deformations are applied. They have allowed the conservation of diatoms over the last tens of millions of years [10,11].

There are two diatom growth environments: deep and shallow. The first is described by high oxygen content, low silica concentration, and planktonic conditions. The second refers to high silica proportion and benthic characteristics. High concentrations of dissolved silicic acid supply nutrients (phosphates and nitrates), which promote diatom development [42]. Planktonic forms float freely, while benthic forms are attached to substrates, rock surfaces, or plants [23].

The amount of light absorbed influences the structure of the frustule. The size and shape of the phytoplankton influence the amount of light absorbed. Small cells are more efficient in absorption than large cells with the same concentration and type of pigment. There are records of species that can grow in the dark [43].

Some diatoms catalyze bicarbonate by protonation in the areas surrounding the cell with low CO_2 contents. The surface characteristics of the frustule can enhance nutrient fixation, as they lengthen the adhesion time in the absorption zone and can even limit the entry of viruses or bacteria. Turbulent flows boost nutrient transport, with elongated cells benefiting more than rounded cells [2].

The availability of nutrients and silicic acid influence the formation of diatoms and their frustules. In nutrient-deficient marine environments, smaller species adapt and grow better than larger species. Frustules with older morphotypes show stronger silicification than those with more recent morphotypes. It is to be expected that older diatoms record higher frustule walls (cross-section) and higher silica per unit area [2].

The frustules are susceptible to dissolution processes, which lead to variations in the contents of silica and carbon. This is associated with the changes that can occur between glacial and interglacial periods. Most of the dissolution occurs in the shallowest part of the water column. The dissolution can be a consequence of taphonomic processes (during its formation stage) or ecological effects (after its formation) [38].

2.2. Diatom Frustules

Diatom frustules originate from a biomineralization process in an ordered, porous silica medium (nanospheres deposited in geometric and dimensional patterns). The frustules help diatoms in functional activities like mechanical stability, virus and nutrient filtration, rate of sinking, and regulation of light entering the cell [2,44].

The structure of the fossils makes it self-supporting, with the minimum content of silica. Frustules must be able to withstand mechanical loads, not only external (predators) but also internal (turgor and reproductive stages) [9].

The liquid-solid phase surrounding the structure and pores of the frustules is of special interest. The diatoms' double external porous layers reduce friction between them and the outer water and increase resistance to liquid pressure. Depending on their morphology, frustules tend to act as self-repairing and self-lubricating media [10].

The size, presence of pores and stiffness are characteristics of the frustules that differentiate them from other inorganic or soil particles with typical diameters between 30 and 100 μm. Diatom-rich sediments exhibit physical properties different from those reported by typical organic and inorganic soils. Conventional geotechnical methods are insufficient to complete their characterization, which is necessary to establish a new type of fossiliferous soil, given their unique behavior [12,13]. Creating a new diatomite classification based

simultaneously on their engineering properties and the biological structure of the frustules is suggested by Ref. [45].

Some frustules extracted from Jawornik (Poland) report cylindrical and centric shapes, variable radii between 50 and 60 µm and porous surfaces. The pore sizes range from 100 to 200 nm. There is no evidence of dissolved silica inside the pores [1]. The content of fossil fragments affects both the fabric and microstructure of the soil matrix containing them and their water retention properties [46].

Diatomite is composed almost exclusively of diatom fossils. It records two types of pores: skeletal pores in the frustules and interparticle pores. Diatomite samples from Oita (Japan) report skeletal pores with diameters generally less than one µm. Centric diatoms of *Cyclotella* species have variable diameters between 20 µm and 40 µm. Centric diatoms present in the clay soils of Osaka in Japan exhibit variable skeletal pore diameters between 0.02 and 1 µm [47].

2.3. Scanning Electron Microscopy as a Technique for the Characterization of Frustules

Scanning Electron Microscopy (SEM) is a technique that allows visualization at small scales, using instruments that apply radiation other than visible light [14]. This microscope does not form an exact image of the object but constructs a virtual image from some of the signals emitted by the sample. If a non-conductive material is observed, it is coated with a thin metallic layer, e.g., gold [14]. Alternative procedures have considered coating samples with resins and subsequently covering them with graphite [17].

The study of materials through SEM consists of amplifying the surface views of the observed structures and examining their properties. The samples are approached using an electron beam generated in a vacuum environment, which is directed with electromagnetic lenses, thus creating high-resolution images. These interactions provide information on topography, morphology, shape, size, composition, and crystallographic structure. The size of the samples must be defined depending on the material, and their surface must be clean. The dimensions of the sample must be adjusted to the chambers of the equipment [15].

An advantage of this technique is the possibility of obtaining information about the mineralogy of the particles since an energy-dispersive X-ray spectrometer (EDS) can be operated simultaneously. By comparing the standard spectrum of each mineral, it is possible to determine its presence within the sample [15,16] if its concentration is higher than 1% [14].

The behavior of some soils, especially fine soils (silts and clays), cannot always be understood from their physical and mechanical properties. In such cases, SEM is necessary to assess the microstructure. SEM is used to understand some soil types' differential or problematic performance, verify upgrading or stabilization processes, and identify cementation and contact structures that may occur around the particles. SEM offers high image resolution, detailed surface topography, ease of use, fast image capture and generation of data in digital format. The main disadvantage is the high cost of microscopy services [15].

This SEM practice in DS is mainly associated with the identification of the species according to morphology, size, pore structure, chemical composition, interaction with other types of particles, state of preservation and arrangement within the soil matrices that contain them [18,19,48–50].

2.4. Mechanical Strength of Diatom Frustules and Atomic Force Microscopy AFM

AFM allows for the obtaining of high-resolution images from changes in the height of surfaces, making it possible to recognize objects at the nanoscale. Studies applying this technique to diatoms have increased significantly since 1992. AFM is applied for studies of taxonomy, biomineral formation, ultrastructure, mucilaginous layers, defor-

mation, adhesion, Young's modulus, and nano and micromechanical properties, among others [20,21].

An AFM consists of a micromachined elastic cantilever with a sharp tip perpendicular to the cantilever. When a force is applied to the tip, the cantilever deflects proportionally. The cantilever should have a sufficiently low "spring constant k" so that large deflections can be obtained when small forces are applied. These deflections are detected by a laser system reflecting on the cantilever. The AFM is suitable for studies in humid environments (water or other solutions). In addition to imaging, stress and strain records can be obtained from the AFM, even on a single-molecule scale [23].

The advantages of AFM over SEM microscopy are high image resolution, 3D representation, and the possibility of measuring physical and structural properties in a desired spatial environment. The accuracy of the quantitative results of nanoindentation and elastic measurement of AFM has been the subject of discussion, but the relative micromechanical information still turns out to be of great importance [22].

Concerning diatoms, AFM has been implemented from two perspectives. The first involves the total assessment of the cell through the progressive application of loads on its frustule, up to the point of reaching breakage. The second corresponds to evaluating the local properties, i.e., the resistance of the elements that make up the structure. The modulus values obtained in various investigations (for the few species studied) have shown considerable differences, even of an order of magnitude. This situation is associated with the variation in the silicification levels and the conditions of execution of the measurements [51].

Another line of research has been the nanoindentation of the surface, from which the results of depth and area make it possible to calculate the hardness of the frustules. This magnitude is a function of the geometry of the indenter. It is not always possible to differentiate whether the results of an indentation correspond exclusively to local properties (elastic deformations) or whether the influence of the total geometry of the frustule is present [22].

Although current technological advances do not allow the development of artificial siliceous structures with the level of precision and ordering (hierarchical structure) that diatoms do, nor do they allow the reproduction of the stages of biomineralization, atomic force microscopy at least opens the possibility of studying these organisms "in vivo", with a high level of spatial resolution and with the possibility of evaluating the mechanical behavior of both the frustules and the adhesive substances excreted [23,52].

Ref. [48] used AFM to investigate the nanostructure, morphology, physical properties and the relationship of the outermost organic layer to the silica frustule under natural hydration conditions. AFM images revealed that the silica walls are coated by a thin mucilaginous material covering most of the surface, which is non-adhesive, soft, non-soluble and compressible.

From the AFM on the diatoms of the *P. viridis* species, it was recognized that the frustules are composed of packed silica spheres with diameters close to 44.8 nm in the valves and 40.3 nm in the bands. For the species *Hantzschia amphioxys*, spheres with sizes close to 37.1 nm in valves and 38.1 in bands were found. It can be concluded that the sphere size does not change significantly between the place of arrangement within the same frustules, whereas the change is considerable when the species varies [48]. Another element of interest was the identification of pores between the silica spheres, i.e., the packing of the spheres inside the frustules is not fully dense, which opposes the assumption of high solidification calculated from deflection tests. The tests by [48] were performed on diatoms in natural conditions, i.e., without removing or cleaning the external mucilaginous layer. Therefore, the results obtained involve the whole system (silica frustule + organic coating),

which is why the AFM experimentation could not distinguish the mechanical contributions of each layer.

Different sample preparation processes must be applied to visualize diatoms and assess frustules in the AFM. These cells can be analyzed in dry or wet environments. Sample preparation techniques may include oxidation procedures of the organic material covering the cell or its coating prior to observation. If the organic components are not cleaned, many details can be darkened. However, it is essential to consider that some diatom species with low silica content may collapse during sample preparation. AFM resolution is reduced because of scattering generated by mucilaginous organic coverage, mainly when sensitive tip methods are applied in liquid environments [22].

Ref. [52] have implemented AFM microscopy to observe living diatoms and follow their growth stages, to recognize the topography of their frustules, to determine the thickness of the organic coatings (ranging in the range of 10 nm), to observe biomineralization processes and to record the movements of these organisms, as well as the formation of chains. The production of binders that allow cells to adhere to substrates or other diatoms has been recognized as efficient in permanent submersion conditions in fresh and salty environments. Most manufactured adhesives lose their properties upon contact with humid environments as they undergo chemical changes that detach them from the substrate or the environment that supports them [23].

Ref. [53] evaluated the topography and mechanical properties of adhesive substances secreted by two species of diatoms through their pores or "Raphe". The observations determined that, in both species, the secretion covers almost the totality of the frustules. From the force curves, it was possible to calculate the adhesive strength, around 3.8 nN. For the particular case of secretions through the "Raphe" in the form of strands or fibers, breaking strengths as high as 60 nN were reported. Diatoms may have multiple mechanisms for producing organic coatings on the cell surface [49].

Ref. [23] studied natural adhesives from diatoms of the *Eunotia sudetica* species. This species was selected considering its size (tens of microns) and ease of micrometric manipulation. These organisms were cultured in controlled fluid environments and subsequently self-adhered to glass slides. The analysis focused on the force-distance curves obtained from the adhesion zone of the cells to the glass substrate. From the loading and unloading application cycles, it was concluded that the adhesive force increases with extension. Suppose the load is removed after an adhesive breakage (separation of the cell from its substrate), and contact is regained. In that case, the adhesive properties are recovered, provided that a continuous interaction is allowed for more than 30 s.

Ref. [24] reports that the C_S recovery rates obtained in a one-dimensional consolidation test on diatomaceous soil are up to twice as high as those recorded for kaolin-type soil. This phenomenon can be associated with the elastic properties of diatom frustules. Ref. [24] apud [11] points out that diatoms are not entirely rigid and show considerable elastic deformation before breaking. This conclusion results from multiple tests performed on frustules subjected to loads through AFM.

This leads to a comparison of the elastic recovery obtained in atomic microscopy (particularly when the loads are removed) with the elastic rebound observed in one-dimensional consolidation tests when the vertical stresses are removed in the unloading stage. This aspect applies to both intact and fractured frustules. Diatom-rich sediments can thus "remember" the in situ stress regime. However, these soils are not cohesive and can quickly lose or acquire water, which generally disturbs the samples and leads to stress memory loss [24].

Ref. [11] assessed the defensive capacity of the frustules as diatom armor against possible attacks by predators through the quantification of their mechanical resistance. Virtual

(finite element analysis) and accurate load tests by atomic force microscopy using calibrated glass microneedles were carried out on a series of centric and pennate cells. The forces required to rupture live and individual cells of three diatom species, *Thalassiosira punctigera*, *Coscinodiscus granii* (centric) and *Fragilariopsis kerguelensis* (pennate), were measured. All species' shear strength was inversely proportional to diameter (See Table 1).

Table 1. Forces to induce breakage in diatom frustules of different species.

Species	Type	Tool of Force Application	Reference Dimension (μm)	Breaking Strength (μN)	Young's Modulus (GPa)
Thalassiosira punctigera	Centric	Calibrated glass microneedles	50	260	22.4
Thalassiosira punctigera	Centric		100	180	
Coscinodiscus granii	Centric		130	90	
Fragilariopsis kerguelensis	Pennate		30	730	

Modified from [11].

From the previous results and finite element simulations, it was deduced that the ultimate compressive and tensile strength depends on the place where the force is applied, either on the faces or on the lateral bands. The latter presented the highest resistant stresses (up to 680 N/mm^2) [11].

The behavior during the application of the loads indicated that the frustules presented rigid failure. Verifications of fractures in pennate diatom frustules have shown that the crack path does not pass through but surrounds the silica spheres that form the frustule, leading to a greater separation length and energy required to generate the breakage [11].

Frustules perform several functions in diatoms, one of which is to provide mechanical stability. The presence of pores and ridges decreases the concentration of stresses on the frustule's structure. Through atomic force tests, it has been found that these elements can withstand stresses ranging from 1 to 7 N/mm^2 (100–700 t/m^2) [11,44].

From nanoindentation tests, different moduli of elasticity were obtained in frustules of *Coscinodiscus* species, which ranged from 3.40 to 15.61 GPa, Refs. [10,54]. The micromechanical properties of the frustules show significant variations depending on the layer that was analyzed. "A clear correlation between mechanical properties and diatom features (e.g., porosity, shape, thickness and pore size) has not yet been established" [55].

Ref. [56] studied the flexibility of four morphologically different diatom species. The flexural rigidity varies widely, even up to four orders of magnitude (1.7×10^{-13}–1.3×10^{-17} Nm^2). Ref. [22] reports hardness values in diatoms of the species *Navicula pelliculosa* between 1 and 12 GPa, although higher values are referenced in certain places of the frustule.

Ref. [21] analyzed the changes in the mechanical properties and the impact on the population of some freshwater diatoms due to variations in environmental conditions (water acidity and temperature). Nanomechanical assessment was conducted using an atomic force microscope in a peak force touch mode. For the case of *Cyclotella meneghini* species, Young's modulus values were recorded in the frustules, between 7 and 25 GPa.

Ref. [51] developed micro indentation experiments using the AFM to evaluate the local variations of Young's modulus in both cells and junction structures that are part of diatom chains of marine origin of the *Lithodesmium undulatum* species. From the results, it was possible to recognize the significant variability of the modulus and determine that the components of the frustule that are newly formed are softer than those associated with the parental cells. The hardening of the new parts may involve the incorporation of organic material. However, further studies are needed to elucidate the mechanical properties of the frustules from the cell formation cycles.

Table 2 presents the reference values presented by Ref. [51], complemented by a review of the state of the art in relation to Young's Modulus.

Table 2. Young's Modulus Register for different diatom species.

Species	Young's Modulus	Cantilever Tip	Dimension	Spring Constant	Remarks	Ref.
Navicula pelliculosa	15–30 GPa Central rib 40–100 GPa Central rib 30–100 GPa Central node	Conic	Nominal radius 25 nm Spherical indenter Outer radius 10 nm	294 N/m 143 ± 2 N/m 24.4 N/m	Artificial freshwater culture. Tests developed on dry samples. Preparation and visualization of samples by two methods (mechanical transfer and surface growth with subsequent ethanol washing).	[22]
Coscinodiscus	1.7–15.61 GPa	Conic	Nominal radius 25 nm.	132 N/m	Treatment with sulfuric acid to remove organic matter.	[10] [54] [51]
Phaeodactylum tricornutum	0.25–0.75 MPa 500 kPa ovoid-shaped valves 100 kPa other valve shapes.	Conic	Nominal radius 20 nm	0.01 N/m	Live cells in NaCl solution.	[57] [51]
Cylindroteca closterium	2–5 MPa 43.7 MPa on silica bands 21.3 MPa between silica bands 29.8 MPa mean value in the valve	Conic	Nominal radius 8 nm	5 N/m	Living cells in seawater. Acid treatment.	[58]
Lithodesmium undulatum	0.25–9 MPa 729 kPa 737 kPa 3.2 MPa 2.3 MPa	Spherical Spherical Spherical Spherical Spherical	2 µm 2 µm 2 µm 2 µm 2 µm	4.5 N/m 4.3 (±0.2) N/m 4.3 (±0.2) N/m 4.3 (±0.2) N/m 4.3 (±0.2) N/m	Living cells in seawater. Silicon nitride cantilevers. Living cell, marginal ridge, cell division during incubation. Living cells, valve, and cell division during incubation Living cells, marginal ridge, No cell division during incubation. Living cells, valve, No cell division during incubation.	[51]
Thalassiosira punctigera	22.4 GPa				Cells were cultured at 15 °C and moderate light intensity. Tests carried out in seawater environment. Loading application with calibrated glass microneedles.	[11]
Cyclotella meneghini	7–25 GPa				Freshwater diatoms. AFM is applied with "Peak Force" contact method.	[21]
Coscinodiscus	1.1–10.6 GPa	Diamond Berkocvich	20 nm	42 N/m	Central marine species. Clean diatom sample mounted on a glass sheet with an adhesive solution. Resonant frequency of 300 kHz in intermittent contact. Pretreatment with nitric acid and ethanol.	[55]
Synedra	13.7–18.6 GPa	Diamond Berkocvich	20 nm	42 N/m	Pennate marine species. Clean diatom sample mounted on a glass sheet with adhesive solution. Resonant frequency of 300 kHz in intermittent contact. Pretreatment with nitric acid and ethanol	[55]

The elasticity of the frustule is variable depending on the place where it is evaluated and the level of silicification. The "girdle" region, in fusiform and ovoid species, can report values up to five times lower than in the valves. The arms of triradiate species are softer than their core. A silicified frustule in ovoid species is five times more rigid

(Young's Modulus values up to 500 kPa) than the components of a diatom that has not been silicified [20,57].

Indentation tests on diatom frustules of the *Coscinodiscus* species by modifying the angles of incidence and the location point are reported by refs. [55,59]. The fossils' elastic modulus (E) and hardness (H) were calculated.

The mechanical properties were defined mainly by the point of load application and not so much by the size of the frustule. The values ranged E: 0.59–2.77 GPa and H: 0.03–0.12 GPa in the center of the frustule. The reports obtained were complemented with simulations by the Finite Element Method, finding good agreement.

Ref. [60] reports Young's modulus values for different regions of diatom frustules (biogenic silica); thus, transapical rib (7–20 GPa), central rib (15–100 GPa), central nodule (30–100 GPa). Simultaneously, it reports values for synthetic silica between 66.3 and 74.8 GPa. The authors associate these values with the material's low density (2.2 g/cm^3).

In addition to studying the mechanical properties of frustules, atomic force microscopy has been applied to the statistical study of the morphology of fossils in aspects such as geometric conditions, pore size distribution, and height variation in different places of the fossil, among others [45].

3. Materials and Methods

The materials and procedures applied during the investigation are described below. Emphasis is placed on the characterization of diatomaceous soils using SEM, XRD, and AFM procedures.

3.1. Diatomaceous Soils

The particles analyzed are frustules from diatomaceous soils located in Colombia, Mexico, and Peru. These were selected due to their evident morphological differences, a product of visualization through the Scanning Electron Microscope (SEM). The inputs were obtained from mining deposits, crushing diatomites, and marketing them as agricultural amendments, insecticides, or filter layers. The recognition of the species and the morphology of the frustules analyzed are shown in Figures 1–4.

The scanning electron microscope is a Carl Zeiss Evo HD 15, with a LaB6 (lanthanum hexaboride) emitter, using Smart SEM software version 5.07. The X-ray energy dispersive spectroscopy (EDS) detector, an Oxford Instruments X-max 20, uses AZtec 3.0 SP2 software. The metallizer for the samples is a Quorum Q150R ES.

The EDS tests were executed with the SEM. The multiple observations considered the following configuration: livetime (s): 30.0–181.9; process time: 2; Accelerating Voltage (kV): 15.0; Magnification: 1600X; Working Distance (mm): 8.3–8.8; Elevation (degrees): 35.0; Number Of Channels: 2048; Energy Range (keV): 20; Energy per Channel (eV): 10.0; Detector Type: X-Max; Window Type: SATW.

The chemical composition of the frustules (presence of minerals or compounds) was studied by Energy Dispersive Spectrometry (EDS) and X-ray diffraction (XRD). From the former, peaks of Oxygen and Silica could be recognized in the three species. Other elements such as Aluminum, Sodium, and Carbon were identified, but in minimal concentrations. See Figure 2.

From the XRD tests conducted on samples from three different sources, peaks matching silicon dioxide SiO_2 were detected. This description aligns with the characteristics of amorphous hydrated silica and pure biogenic opal. Please refer to Figure 3.

The diffraction tests (XRD) were carried out with a Malvern-PANalytical model Empyrean 2012 brand equipment, with a Pixel 3D detector and a Cu source ($\lambda = 1.541$) at 45 kV and 40 mA. Goniometer: Omega/2 theta. Platform Configuration: The reflection

Transmission Spinner is rotating at 4 rpm. The step was 0.03°, and the time per step was 50 s. Identification was performed using High Score Plus software and the Rietveld method. Database: ICSD FIZ Karlsruhe 2012-1.

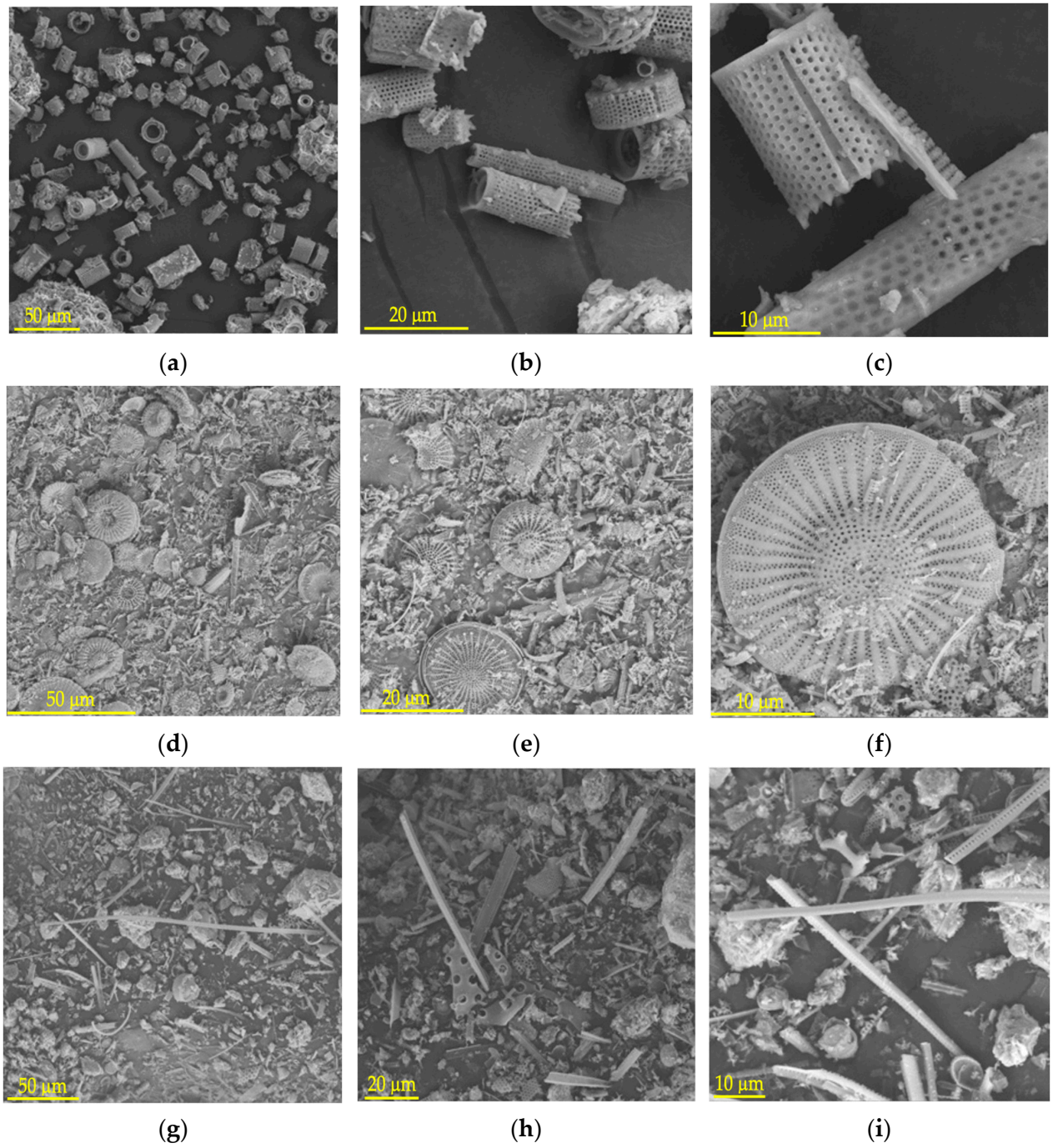


Figure 1. Identification of species employing SEM. (**a**–**c**) Colombia (Boyaca)_Aulacoseira Granulata _Centric monospecies, cylindrical; (**d**–**f**) Mexico (Jalisco)_Cyclostephanos tholiformis_Centric monospecies, disc shape; (**g**–**i**) Peru (Ica)_Thalassionema nitzschioides_Elongated, symmetrical shapes. Colombian species Length (µm): 5.19–38.66; Diameter (µm): 4.04–23.97_Mexican species Diameter (µm): 3.09–28.52_Peruvian species Width (µm): 0.96–5.42.

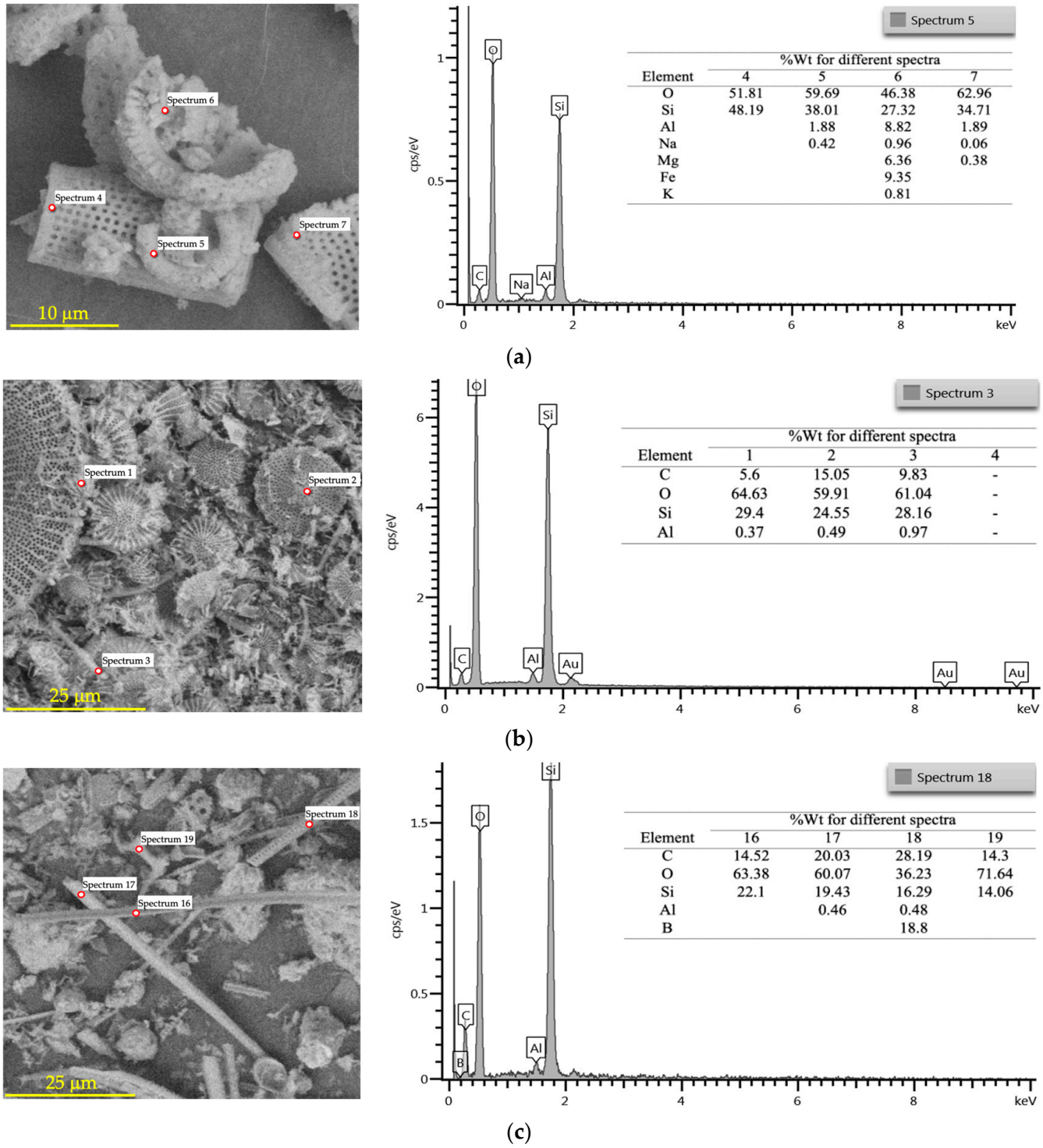
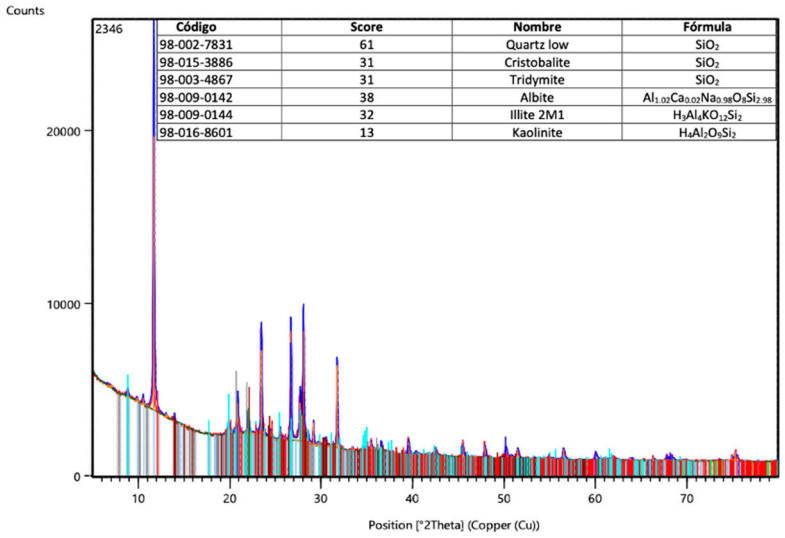
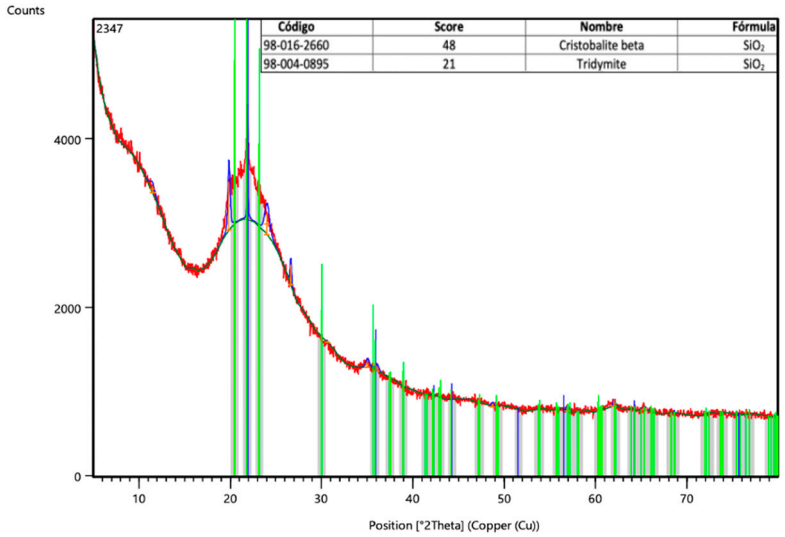


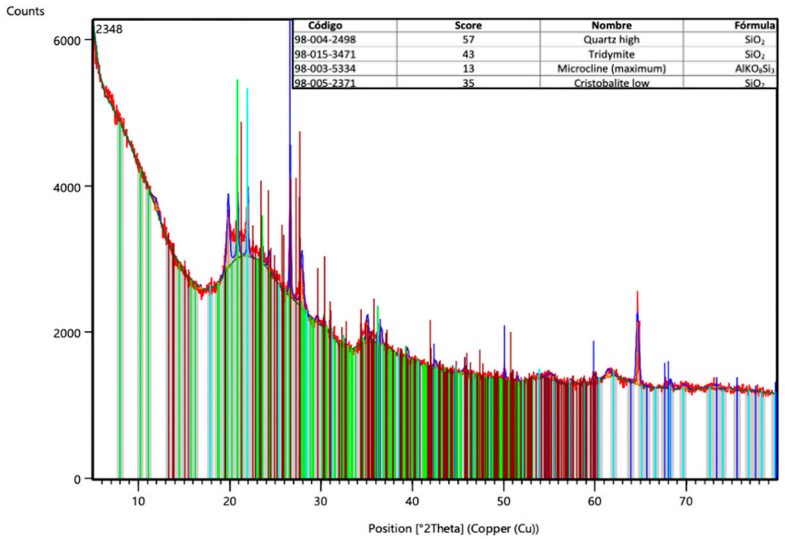
Figure 2. Mineralogical identification by EDS in frustules of different diatom species (**a**) Colombia_Aulacoseira Granulata; (**b**) Mexico_Cyclostephanos tholiformis; (**c**) Peru_Thalassionema nitzschioides.



(**a**)



(**b**)



(**c**)

Figure 3. XRD characterization of frustules of different diatom species. (**a**) Colombia_Aulacoseira Granulata; (**b**) Mexico_Cyclostephanos tholiformis; (**c**) Peru_Thalassionema nitzschioides.

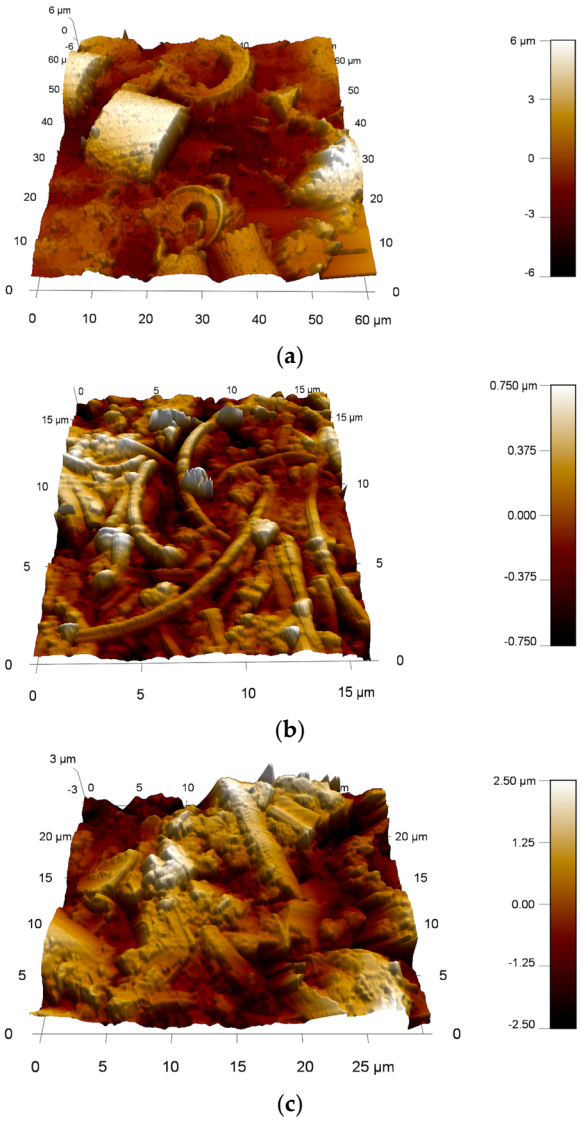


Figure 4. 3D representation of species by means of AFM (**a**) Colombia_Aulacoseira Granulata; (**b**) Mexico_Cyclostephanos tholiformis; (**c**) Peru_Thalassionema nitzschioides.

3.2. Sample Preparation and Application of Forces in AFM

The preparation involved suspending 0.5 g of each diatomaceous earth in deionized water. The mixture was then exposed to an ultrasonic bath for 30 min to ensure complete dispersion. Subsequently, the sample was placed on a glass substrate and allowed to dry at room temperature.

Atomic Force analysis was performed using the Oxford Instruments MFP-3D Asylum Research reference equipment. Imaging was carried out in "intermittent mode", with an oscillation frequency of 82 kHz and a scanning speed of 0.35 Hz. See Figure 4. The "force curve mode" was used to analyze the mechanical properties, employing a spherical tip made of silicon, denoted as AC240 TS, with a radius of approximately 10 nm. The cantilever used had a stiffness of 4.39 nN/nm. The curves obtained were fitted to the "Hertz contact model", from which Young's modulus (E) records were obtained.

Despite its limitations, the Hertz model is widely used for the nanomechanical characterization of samples in contact or impact conditions [61]. This model does not account for the viscoelastic properties of biological samples, the sample's dimensions, and the substrate's effects, thereby leading to inaccuracy in large deformations [62]. The selection of a particular model will depend on the indenter geometry and the sample surface. The

most commonly used model for the micromechanical analysis of biomaterials is the Hertz model [63].

The Hertz model considers the sample as an isotropic linear elastic solid that extends infinitely and assumes that the indenter is non-deformable. The equation to be implemented is determined by the geometry of the indenter. This model is suitable for analyzing indentations that are small (5% to 10% of the sample height) and where the substrate has no influence. Under these conditions, the calculation of Young's modulus is possible [63–65].

The mathematical support for calculating the "Young Modulus" is presented below. The most common models for spherical indenter are given depending on contact radius and Poisson's ratio.

$$F = \frac{E}{(1-\nu^2)}\left[\frac{a^2+R^2}{2} ln\frac{R+a}{R-a} - aR\right] \quad (1)$$

F: Force
E: Young Modulus
ν: Poisson's ratio
a: Radii of the contact circle
R: Radius of the sphere [64]

$$F = \frac{E}{2(1-\nu^2)}\left[\left({r_c}^2+R^2\right) ln\frac{R+r_c}{R-r_c} - 2r_cR\right] \quad (2)$$

F: Force
E: Young Modulus
ν: Poisson's ratio
r_c: Contact radius
R: Spherical indenter radius [62]

$$F = \frac{4E}{3(1-\nu^2)}\sqrt{R\delta^{3/2}} \quad (3)$$

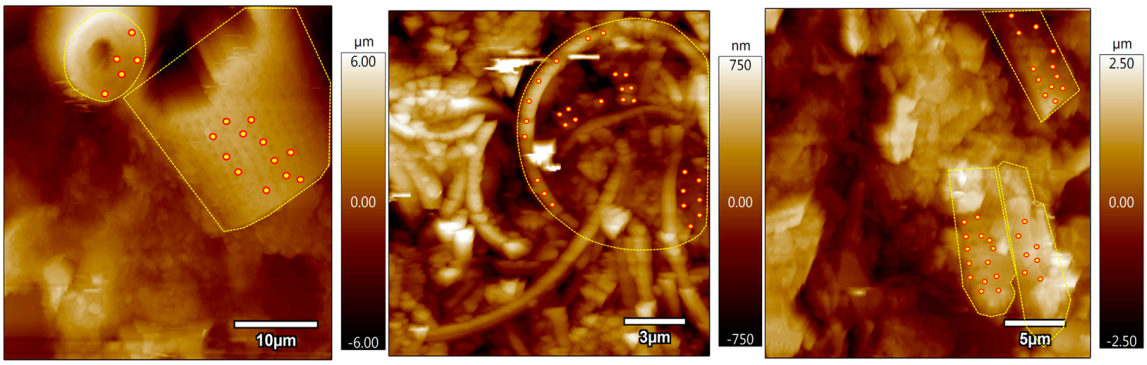
F: Force
E: Young Modulus
ν: Poisson's ratio
δ: Indentation depth
R: Spherical punch tip radius [22]

4. Results and Discussion

The results focus on the presentation and comparative analysis of the "force—deformation curves" of the three species studied, obtained from the AFM tests. This depends on the places where the loads are applied. In addition, the AFM curves of other diatom species generated by reference authors are contrasted. Finally, Young's modulus values are recorded for the different types of frustules, taking into account the point of application.

4.1. Force—Deformation Curves

The forces were applied at different points on the frustules, chosen based on the morphological characteristics of each species. In the Colombian sample, the main ring and the cylinder wall were targeted. For the Mexican sample, the forces were applied to the rim and the center of the plate. In the case of the Peruvian sample, due to the elongated shape of the particles, the forces were distributed between the edges and the center. Figure 5 illustrates the locations where the loads were applied.



(**a**) (**b**) (**c**)

Figure 5. Identification of species and load application points by means of AFM. (**a**) Colombia (Boyaca)_Aulacoseira Granulata_Centric monospecies, cylindrical; (**b**) Mexico (Jalisco)_Cyclostephanos tholiformis_Centric monospecies, disc shape; (**c**) Peru (Ica)_Thalassionema nitzschioides_ Elongated, symmetrical shapes.

The force-displacement curves obtained for each of the species are shown in Figure 6.

The curves obtained under the same conditions (species and area of application) were grouped and plotted to compare the results of the different samples. See Figure 7.

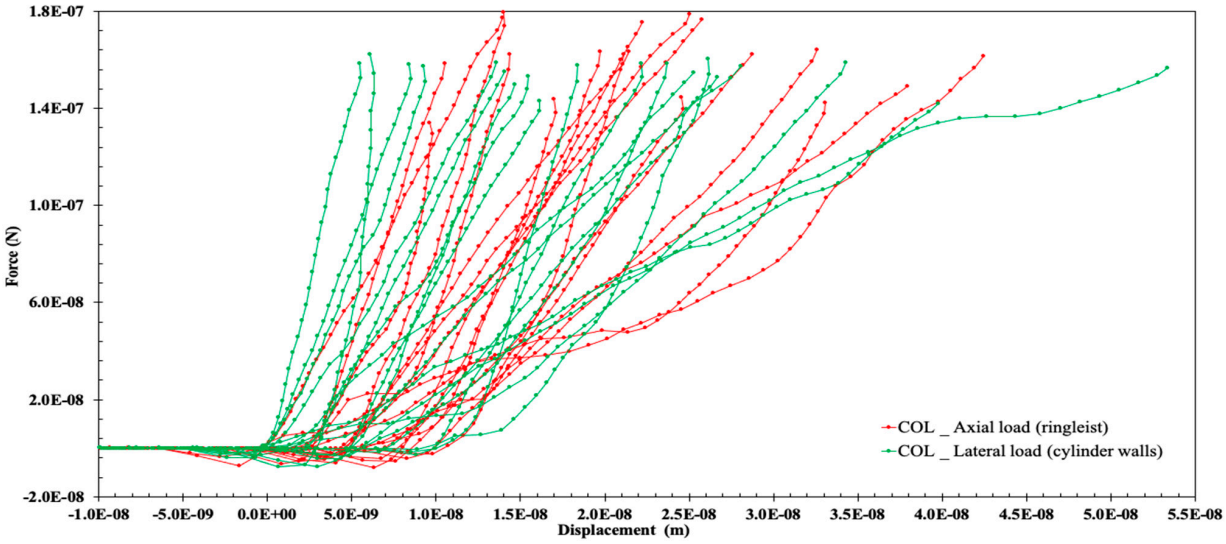
In Figure 7, it is evident that the Mexican species exhibited the highest displacement values and the greatest dispersion, especially when the load was applied on the outer edge. Even when the force was applied to the inside of the radial striae, the displacement still exceeded that reported by the other species under any condition. On the other hand, the Peruvian species displayed the highest concentration and uniformity in displacement. The Colombian frustules showed similar displacement when a load was applied to the cylinder walls or to the ringleist. Interestingly, the maximum applied force values across the three species and different application points were consistent, ranging from 1.4 to 1.8 $\times$ 10^{-7} N.

From Figure 7, it is possible to elucidate that the dispersion is more significant in terms of deformation than force. The uniformity of the results of the Peruvian species is outstanding and can be understood by the more straightforward geometric shape, with a smaller quantity and size of pores than in the other species; this is then associated with greater regularity in the fixation of silica, and in the way, the stresses are transmitted within a medium with fewer discontinuities.

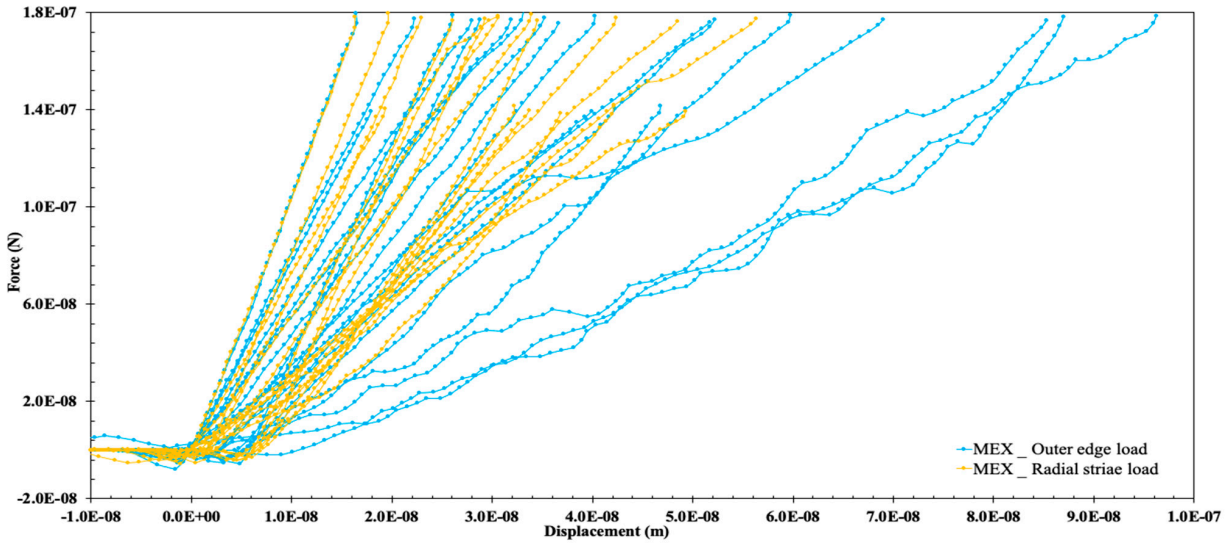
The Colombian species turns out to be quite porous, as much as the Mexican one. However, it registers better behavior in terms of deformations since the cylindrical shape gives it a space of continuity through which the stresses can be dissipated. On the contrary, the Mexican species exposes clear limits on the outer edges where stresses are concentrated.

Figure 3 allows us to recognize that the mineralogical composition of the three species is similar, recording the presence of SiO_2 in all cases, particularly Tridymite and Cristobalite. The shape of the frustules and the organization of the silica spheres will then determine the differential behavior between species. This aspect invites the development of microscopic visualizations at higher levels, in which the organization of the mineral and its arrangement around pores or irregularities can be validated.

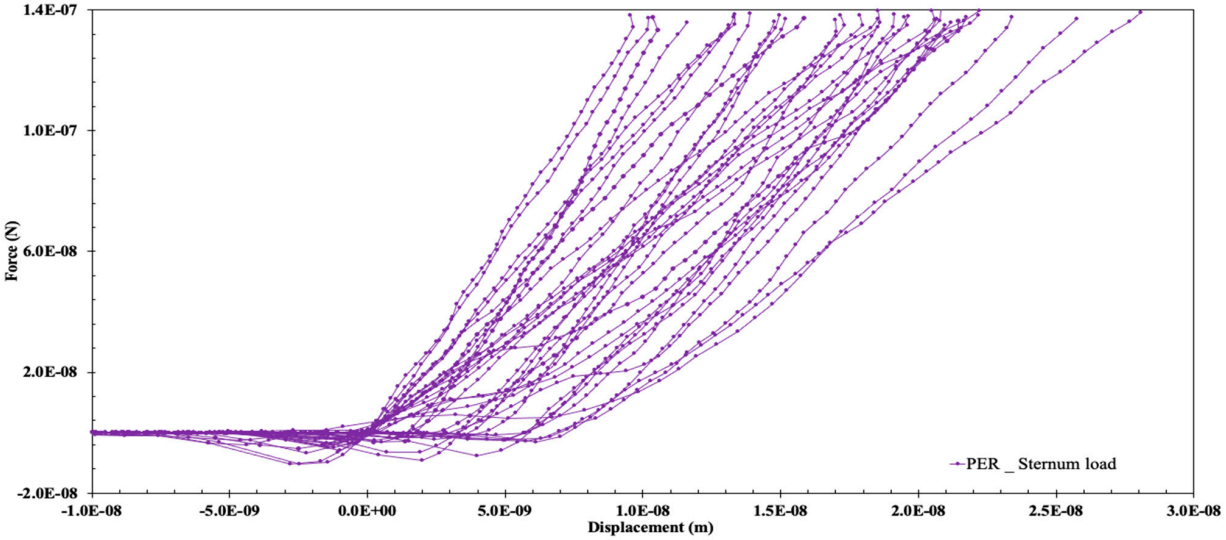
Subsequently, to confirm the reliability of the results, the group of Force-Displacement curves (MEX_outer edge load) was compared with data from other researchers who had applied loads using AFM to diatoms, whether on the frustules, their organic coverings, or the substances they excrete. See Figure 8.



(**a**)



(**b**)



(**c**)

Figure 6. Force-displacement curves obtained by AFM for different species. (**a**) Colombia Aulacoseira Granulata; (**b**) Cyclostephanos tholiformis; (**c**) Perú Thalassionema nitzschioides.

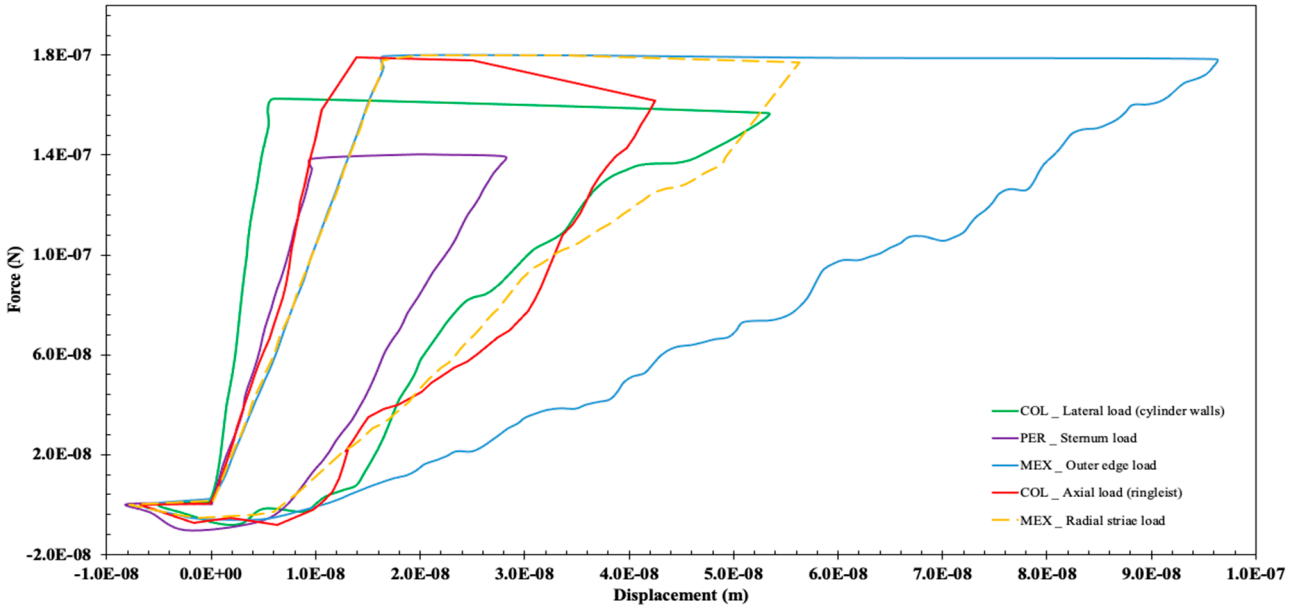


Figure 7. Block contrast of force-displacement curves for different species.

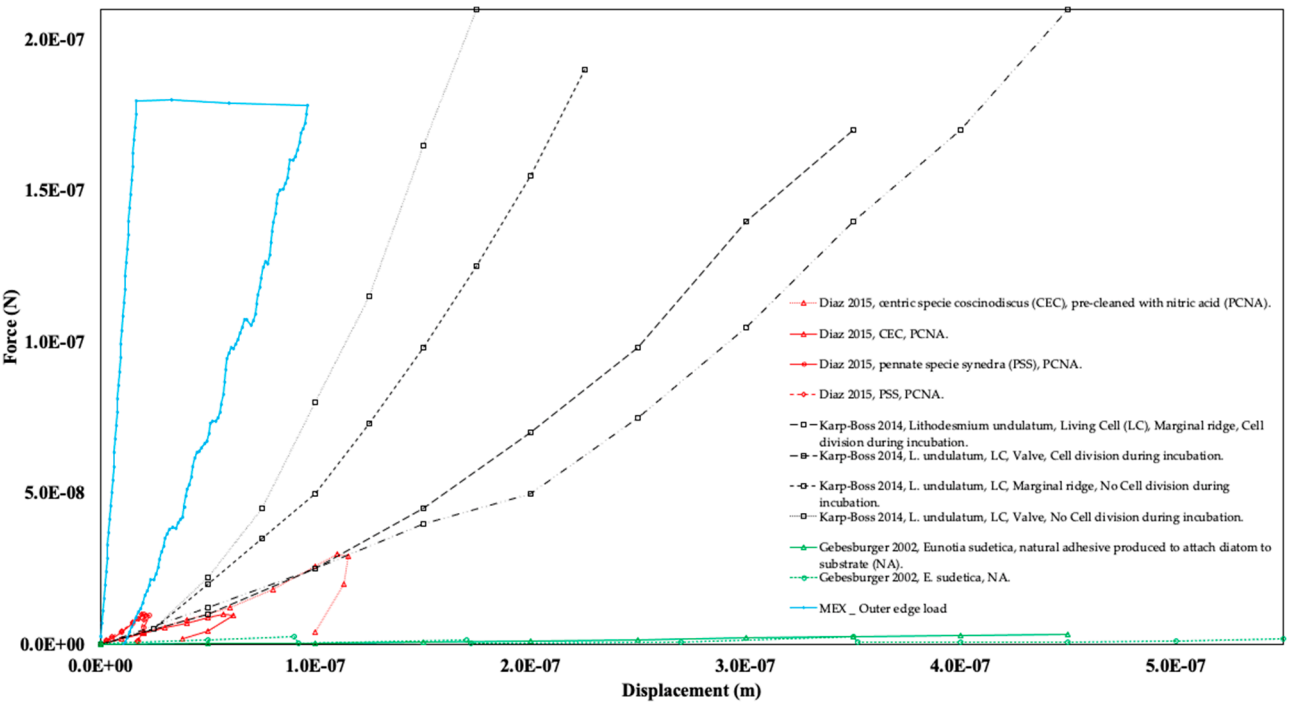


Figure 8. Contrast of force-displacement curves obtained by AFM on frustules or their derivatives [23,51,55].

Regarding Figure 8, the Force-Displacement profiles of the frustules examined in this study exhibit a higher degree of uniformity compared to those documented in previous research, wherein loads were applied to different species, either directly on the frustule or on the derived substances. The force exerted by the adhesive substances expelled by the diatom is significantly lower than the force sustained by the silica structures.

4.2. Young's Modulus Determination

Upon analyzing the curves and incorporating the Hertz model with considerations for the tip geometry, Young's moduli were determined for each species and categorized according to the load application zone. These results are presented in Table 3, revealing

that the species from Mexico exhibit the lowest modulus values, the Colombian species display the highest, and the Peruvian species demonstrate the most consistent behavior. This pattern is akin to the concentration of force-displacement curves observed in Figure 7.

Table 3. Record of Young's Modulus as a function of species and load application zone (MPa).

	Colombian Species		Mexican Species		Peruvian Species
	Axial Load (Ringleist)	**Lateral Load (Cylinder Walls)**	**Outer Edge Load**	**Radial Striae Load**	**Sternum Load**
	596.76	638.97	181.90	219.40	586.19
	320.91	94.66	330.60	193.48	292.03
	1150.00	211.75	165.80	357.23	325.94
	118.94	676.42	156.22	277.09	509.34
	323.40	231.76	49.81	84.46	301.58
	586.83	524.96	101.40	125.70	511.34
	650.62	211.18	156.92	109.41	279.86
	314.68	940.02	159.20	478.50	275.76
	251.94	293.57	490.20	80.37	332.38
	129.84	589.67	40.85	226.30	485.53
	1330.00	479.52	88.09	109.16	484.02
	1260.00	607.84	77.99	114.56	848.90
	1160.00	74.47	350.50	304.36	671.83
	1250.00	602.18	179.09	155.24	403.60
	142.86	1540.00	40.11	334.16	510.56
	393.44	1100.00	98.33	184.33	364.45
	415.92	953.69	148.77	420.18	801.96
	977.60		307.47	372.39	629.45
	121.13		41.62	16.28	366.70
	1030.00		236.30		449.19
			25.12		789.37
			63.38		248.38
			14.25		596.69
			24.67		487.78
			70.88		293.38
			84.85		314.19
			223.52		848.64
			251.67		702.07
					523.88
					326.17
					818.42
					580.03
					435.55
Average	626.24	574.74	148.55	219.08	496.82
Standard Deviation	438.17	391.64	116.48	129.62	184.88
Variability Coefficient	69.97%	68.14%	78.41%	59.17%	37.21%

In terms of the average value of Young's modulus, the lowest magnitudes are recognized in the Mexican species, both in the outer edge (148 MPa) and the Radial striae (219 MPa), which is consistent with the blocks of the "force-deformation" curves of Figure 7 that is, the most significant deformations are observed. The Modulus values of the Peruvian species are the most regular, with the lowest coefficient of variability (Cv) of the three species (<38%); its average value (496 MPa) is higher than that of the Mexican species but lower than that of the Colombian species. Although the Colombian species reports the maximum modulus values, 626 MPa (ringleist) and 574 MPa (cylinder walls), it also exhibits low magnitudes that derive in the most evident dispersion of the three samples (Cv > 68%).

Figure 2 shows the sillification level of the frustules (EDS tests in SEM). For the Colombian sample, an average percentage of contents greater than 36.75% are identified,

while the Mexican and Peruvian species report average values of 27% and 17%, respectively. A relationship between the high modulus values of the Colombian species and its Silica content is evidenced.

Figure 9 is a schematic representation of the frustules studied in this research. Their characteristic shapes are highlighted again: cylindrical, plate-shaped, and elongated for the Colombian, Mexican, and Peruvian species. This figure exposes the load application points (where it was physically possible) and the elastic moduli obtained.

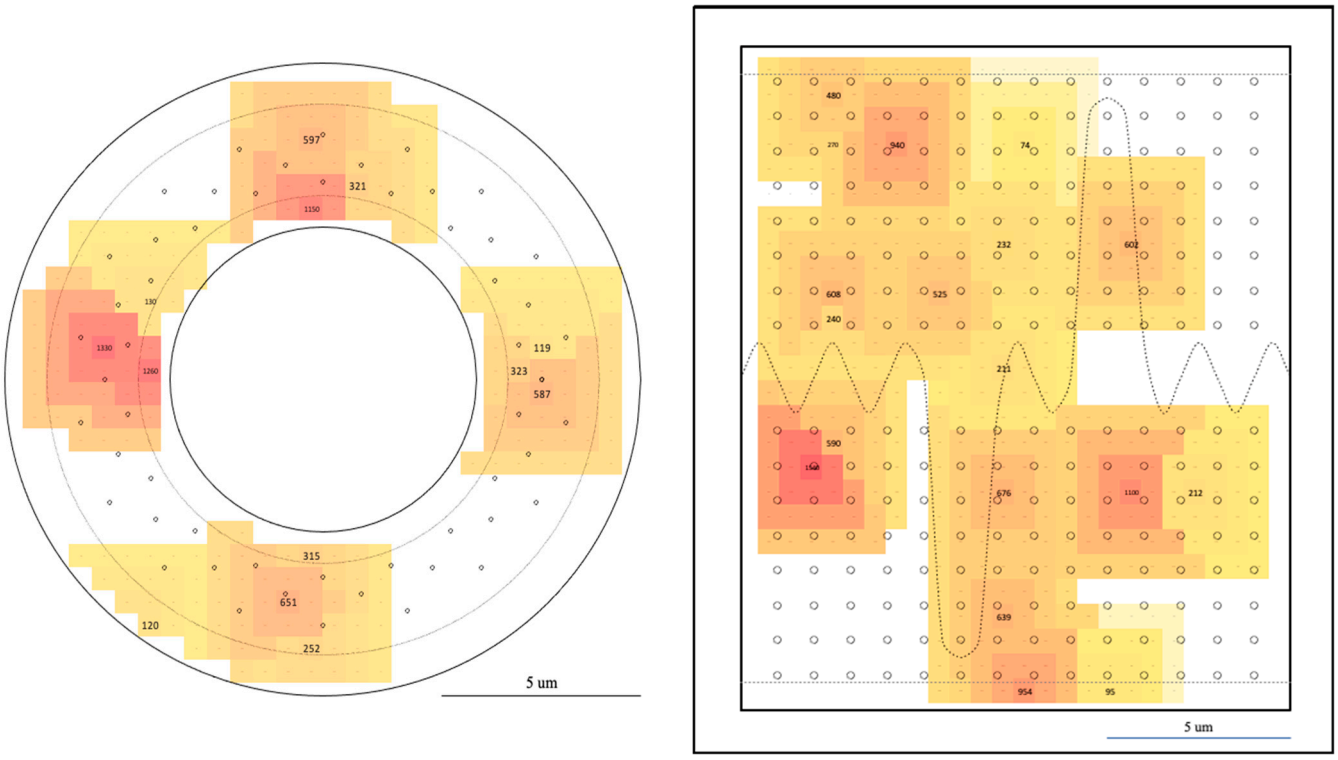
Multiple frustules were analyzed in each species, and the graphic representation corresponded to the superposition of data obtained from the different fossils.

Figure 9 shows that the Colombian frustules Moduli's extreme values (upper and lower peak) are more representative on the lateral faces compared to those obtained in the circular cross-section (ringleist).

In the Mexican species, peak values were obtained in the middle section (over the striae) and the outer ring (outer edge). However, these records are not homogeneous or representative of the entire area; they are specific measurements.

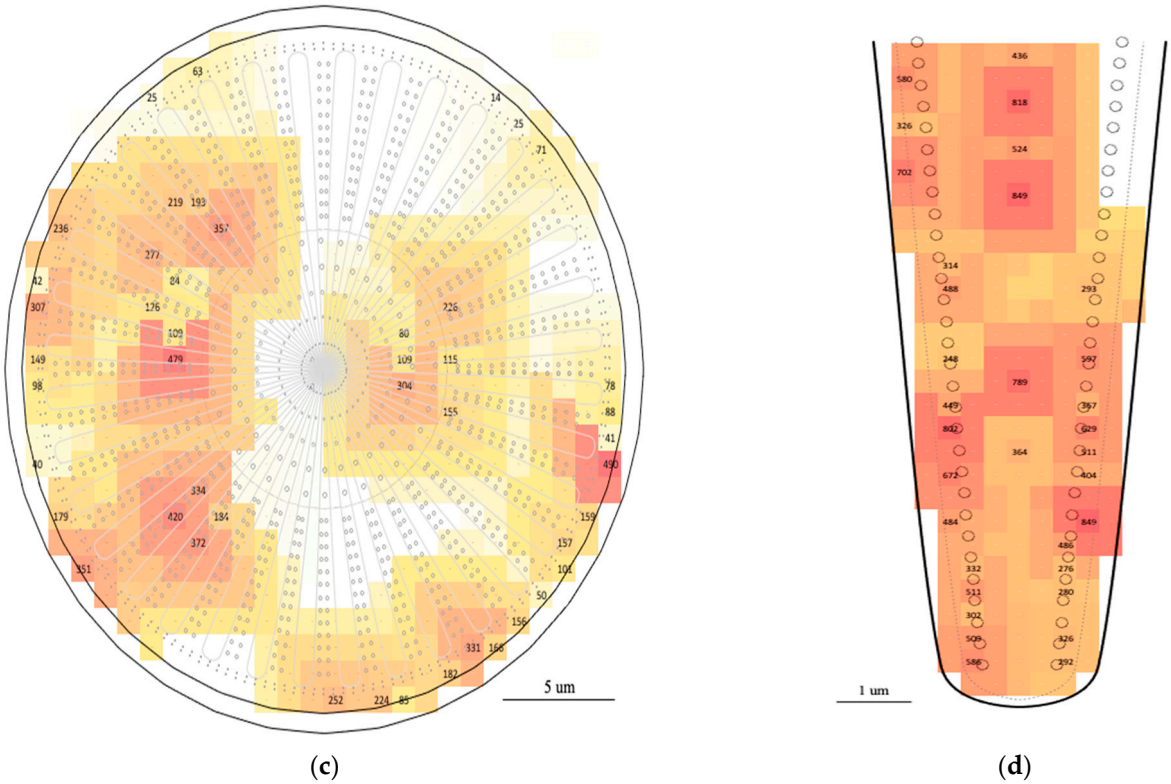
The Peruvian fossil reveals module values that are less dispersed in order of magnitude, which can be understood by the pieces' smaller dimensions (geometric width).

The homogeneity in the results of the Peruvian species is highlighted again; its narrower geometry and lower pore density imply less mechanical variability. It is worth highlighting the geometric differences between the Peruvian and the other two species. In the case of the Colombian species, when applying axial load on the ringleist, higher module values were identified towards the center of the frustule.



(**a**) (**b**)

Figure 9. *Cont.*



(**c**) (**d**)

Figure 9. Modulus of Elasticity (MPa) for different species and load application points. (**a**,**b**) Colombian specie_Axial load (ringleist) and Lateral load (cylinder walls); (**c**) Mexican specie_Outer edge load and Radial striae load; (**d**) Peruvian specie_Sternum load.

5. Conclusions

The atomic force microscopy results obtained in this research are more homogeneous in terms of deformation than the tests developed by other authors on frustules, diatoms, or their organic components.

The load values applied in this research are within the range of variability identified in the background. The loads were not applied until the frustules broke but until the tip generated a stable record. For the local load analysis, the tips were located in whole frustules; application in fragments was avoided. The morphological characteristics of each species defined the load location points.

The XRD and EDS tests revealed that the chemical composition of the three samples is similar regarding the presence of Silica, validating that they are diatom frustules.

The changes in the "force-displacement" behavior are more representative when there is a variation in the type of species and not so much when there is a change in the place of application; this leads to the conclusion that the level of silicification and the growth environment of diatoms are more determining and not so much the morphological organization.

Mexican species exhibited the highest displacement values and the greatest dispersion. The Colombian frustules showed similar displacement when a load was applied to the cylinder walls or to the ringleist. The uniformity of the results of the Peruvian species is outstanding and can be understood by the more straightforward geometric shape, with a smaller quantity and size of pores. This research concluded that the dispersion of results is more significant in terms of deformation than force.

In terms of the average value of Young's modulus, the lowest magnitudes are recognized in the Mexican species. Peruvian species are the most regular. Colombian species report the maximum modulus values and the most evident dispersion.

This research has allowed us to obtain relevant information regarding the mechanical responses of the analyzed frustules of different origins. By understanding the elastic properties and resistance ranges, it is possible to project other types of analysis, such as discrete elements or stress transmission mechanisms, with which the response of the soil mass and not only of a particle could be understood. This information helps determine, for example, yield stresses in fossils, volumetric changes due to their breakage, and the interaction between particles when loads are applied.

Author Contributions: Conceptualization, D.Z.-A. and B.C.-H.; methodology, D.Z.-A. and B.C.-H.; validation, D.Z.-A., J.C.R. and B.C.-H.; formal analysis, D.Z.-A. and J.C.R.; investigation, D.Z.-A.; resources, D.Z.-A. and J.C.R.; data curation, D.Z.-A.; writing—original draft preparation, D.Z.-A.; writing—review and editing, D.Z.-A., J.C.R. and B.C.-H.; visualization, D.Z.-A. and J.C.R.; supervision, J.C.R. and B.C.-H.; project administration, D.Z.-A., J.C.R. and B.C.-H.; funding acquisition, D.Z.-A. and J.C.R. All authors have read and agreed to the published version of the manuscript.

Funding: This work was sponsored with the author's resources, with logistical support from the Nueva Granada Military University and the Universidad de los Andes. The authors' resources are the primary source of financing for the publication process.

Data Availability Statement: The raw data supporting the conclusions of this article will be made available by the authors on request.

Conflicts of Interest: The authors declare no conflicts of interest.

References

1. Lutynski, M.; Sakiewicz, P.; Lutynski, S. Characterization of Diatomaceous Earth and Halloysite Resources of Poland. *Minerals* **2019**, *9*, 670. [CrossRef]
2. Finkel, Z.V.; Kotrc, B. Silica use through time: Macroevolutionary change in the morphology of the diatom fustule. *Geomicrobiol. J.* **2010**, *27*, 596–608. [CrossRef]
3. Gebeshuber, I.C. Biotribology inspires new technologies. *Nano Today* **2007**, *2*, 30–37. [CrossRef]
4. Flower, R.J. *Diatomites: Their Formation, Distribution, and Uses*, 2nd ed.; Elsevier B.V.: Amsterdam, The Netherlands, 2013; ISBN 9780444536433.
5. Arenaldi, G.; Ovalle, C. Compresibilidad y propiedades dinámicas de suelos diatomáceos de Mejillones Compressibility and dynamic properties of diatomaceous soils of Mejillones Introducción Sector de estudio Material de ensayo. *Obras Proy.* **2019**, *25*, 6–14. [CrossRef]
6. Mejía, J.M.; Mejía De Gutiérrez, R.; Montes, C. Rice husk ash and spent diatomaceous earth as a source of silica to fabricate a geopolymeric binary binder. *J. Clean. Prod.* **2016**, *118*, 133–139. [CrossRef]
7. Ficha Técnica. *TIERRA DE DIATOMEAS—AGROPULÍ—TDDA Silicio asimilable: Dióxido de Silicio (SiO2) Amorfo. Enmienda de Uso Agrícola*; Agropuli: Bogotá, Colombia, 2021; pp. 1–13.
8. Al Shatnawi, H.; Bandini, P. Oedometric Behavior of a Diatom-Kaolin Mixture. In Proceedings of the Geo-Congress 2019, Philadelphia, PA, USA, 24–27 March 2019; Meehan, C., Kumar, S., Pando, M., Coe, J., Eds.; ASCE Library: Philadelphia, PA, USA, 2019; pp. 673–681.
9. Sterrenburg, F.; Gordon, R.; Tiffany, M.A.; Nagy, S.; Seckback, J. Diatoms: Living in a Constructal Environment. In *Algae and Cyanobacteria in Extreme Environments*; Joseph, S., Ed.; Springer: Dordrecht, The Netherlands, 2007; pp. 141–172. ISBN 978-1-4020-6111-0.
10. Meng, F.; Gao, G.; Jia, Z. Study on Tribological Mechanism for Multi-layer Porous Structure of Diatom Frustule. *Microb. Ecol.* **2015**, *69*, 45–58. [CrossRef] [PubMed]
11. Hamm, C.E.; Merkel, R.; Springer, O.; Jurkojc, P.; Maiert, C.; Prechtelt, K.; Smetacek, V. Architecture and material properties of diatom shells provide effective mechanical protection. *Nature* **2003**, *421*, 841–843. [CrossRef]
12. Wiemer, G.; Moernaut, J.; Stark, N.; Kempf, P.; De Batist, M.; Pino, M.; Urrutia, R.; Ladrón de Guevara, B.; Strasser, M.; Kopf, A. The role of sediment composition and behavior under dynamic loading conditions on slope failure initiation: A study of a subaqueous landslide in earthquake-prone South-Central Chile. *Int. J. Earth Sci.* **2015**, *104*, 1439–1457. [CrossRef]
13. Locat, J.; Tanaka, H. A new class of soils: Fossiliferous soils? In Proceedings of the XV International Conference of Soil Mechanics and Geotechnical Engineering, Istanbul, Turkey, 1 January 2001; Library of the International Society for Soil Mechanics and Geotechnical Engineering (ISSMGE): Istanbul, Turkey, 2001; pp. 2295–2300.

14. Ipohorski, M.; Bozzano, P.B. Microscopía electrónica de barrido en la caracterización de materiales. *Cienc. Investig.* **2013**, *63*, 43–53.
15. Ural, N. The significance of scanning electron microscopy (SEM) analysis on the microstructure of improved clay: An overview. *Open Geosci.* **2021**, *13*, 197–218. [CrossRef]
16. Igoe, D.; Gavin, K. Characterization of the Blessington sand geotechnical test site. *AIMS Geosci.* **2019**, *5*, 145–162. [CrossRef]
17. Ruge, J.; Palacios, X.; Molina-Gómez, F.; Rojas Suárez, J. Mineralogical, microstructural and porosimetry analysis in three different clayey soils. *J. Phys. Conf. Ser.* **2019**, *1388*, 012014. [CrossRef]
18. Wiemer, G.; Kopf, A. Influence of diatom microfossils on sediment shear strength and slope stability. *Geochem. Geophys. Geosyst.* **2016**, *17*, 1312–1338. [CrossRef]
19. Arenaldi, G.; Ovalle, C.; Barrios, A. Compressibility and creep of a diatomaceous soil. *Eng. Geol.* **2019**, *258*, 105145. [CrossRef]
20. Luis, A.; Hlubikova, D.; Vache, V.; Choquet, P.; Hoffmann, L.; Ector, L. Atomic force microscopy (AFM) application to diatom study: Review and perspectives. *J. Appl. Phycol.* **2017**, *29*, 2989–3001. [CrossRef]
21. Lamczyk, M.; Kawelsky, L.; Noga, T.; Stanek, J.; Berezovska, I.; Berchenko, N.; Parlinska, M.; Cebulski, J. Quantitative imaging of diatoms by PeakForce atomic force microscopy. *Surf. Interface Anal.* **2014**, *46*, 10–11. [CrossRef]
22. Almqvist, N.; Delamo, Y.; Smith, B.L.; Thomson, N.H.; Bartholdson, Å.; Lal, R.; Brzezinski, M.; Hansma, P.K. Micromechanical and structural properties of a pennate diatom investigated by atomic force microscopy. *J. Microsc.* **2001**, *202*, 518–532. [CrossRef] [PubMed]
23. Gebeshuber, I.; Thompson, J.; Del Amo, Y.; Stachelberger, H.; Kindt, J. In vivo nanoscale atomic force microscopy investigation of diatom adhesion properties. *Mater. Sci. Technol.* **2002**, *18*, 763–766. [CrossRef]
24. Wiemer, G.; Dziadek, R.; Kopf, A. The enigmatic consolidation of diatomaceous sediment. *Mar. Geol.* **2017**, *385*, 173–184. [CrossRef]
25. Ponce, J.F.; Fernández, M. Diatom Analysis. In *Climatic and Environmental History of Isla de los Estados*; Springer Briefs in Earth System Sciences: Berlin/Heidelberg, Germany, 2014; pp. 87–104. ISBN 9789400743632.
26. Zepeda, C. *Bacillariophyta Diatomeas Guía Didáctica*; Universidad Autónoma del Estado de México: México City, Mexico, 2019; Volume 1, pp. 1–50.
27. Zahajská, P.; Opfergelt, S.; Fritz, S.C.; Stadmark, J.; Conley, D.J. What is diatomite? *Quat. Res.* **2020**, *96*, 48–52. [CrossRef]
28. Antonides, B.L.E. *Diatomites*; US Geological Survey Publications: Jeffersontown, KY, USA, 1997.
29. Manosalva, S.; Naranjo, W. *Diatomitas. Geología, Caracterización y Potencial Uso Industrial*, 1st ed.; Romero, Y., Ed.; UPTC Publicaciones: Sogamoso, Colombia, 2009; ISBN 9789586601436.
30. Sardo, A.; Orefice, I.; Balzano, S.; Barra, L.; Romano, G. Applied sciences Mini-Review: Potential of Diatom-Derived Silica for Biomedical Applications. *Appl. Sci.* **2021**, *11*, 4533. [CrossRef]
31. Hasan, M.; Saidi, T.; Muyasir, A.; Alkhaly, Y.R.; Muslimsyah, M. Characteristic of calcined diatomaceous earth from Aceh Besar District—Indonesia as cementitious binder. *IOP Conf. Ser. Mater. Sci. Eng.* **2020**, *933*, 012008. [CrossRef]
32. López, J. Comportamiento cíclico de suelos diatomáceos. Master's Thesis, Universidad Nacional Autónoma de México, México City, México, 2009.
33. Lozano, Y. Listado de diatomeas (*Bacillariophyta*) registradas para el mar caribe colombiano. *Bol. Investig. Mar. Cost.* **2010**, *39*, 83–116. [CrossRef]
34. Behrensmeyer, A. Taphonomy. In *Encyclopedia of Geology*, 2nd ed.; Elsevier: Amsterdam, The Netherlands, 2021; pp. 12–22. [CrossRef]
35. Schmid, A. Aspects of morphogenesis and function of diatom cell walls with implications for taxonomy. *Protoplasma* **1994**, *181*, 43–60. [CrossRef]
36. Hildebrand, M.; Dahlin, K.; Volcani, B. Characterization of a silicon transporter gene family in Cylindrotheca fusiformis: Sequences, expression analysis, and identification of homologs in other diatoms. *Mol. Gen. Genet. MGG Vol.* **1998**, *260*, 480–486. [CrossRef] [PubMed]
37. Durkin, C.A.; Koester, J.A.; Bender, S.J.; Armbrust, E.V. The evolution of silicon transporters in diatoms. *J. Phycol.* **2016**, *52*, 716–731. [CrossRef]
38. Warnock, J.P.; Scherer, R.P. Diatom species abundance and morphologically-based dissolution proxies in coastal Southern Ocean assemblages. *Cont. Shelf Res.* **2015**, *102*, 1–8. [CrossRef]
39. Annenkov, V.V.; Danilovtseva, E.N.; Pal'shin, V.A.; Verkhozina, O.N.; Zelinskiy, S.N.; Krishnan, U.M. Silicic acid condensation under the influence of water-soluble polymers: From biology to new materials. *RSC Adv.* **2017**, *7*, 20995–21027. [CrossRef]
40. Thamatrakoln, K.; Hildebrand, M. Silicon uptake in diatoms revisited: A model for saturable and nonsaturable uptake kinetics and the role of silicon transporters. *Plant Physiol.* **2008**, *146*, 1397–1407. [CrossRef] [PubMed]
41. Lewin, J. Silicon Metabolism in Diatoms. *J. Gen. Physiol.* **1955**, *39*, 1–10. [CrossRef]
42. Avramenko, A.S.; Cherepanova, M.V.; Pushkar', V.S.; Yarusova, S.B. Diatom characteristics of the Far East siliceous organogenic deposits. *Russ. Geol. Geophys.* **2015**, *56*, 947–958. [CrossRef]

43. Pahl, S.L.; Lewis, D.M.; Chen, F.; King, K.D. Heterotrophic growth and nutritional aspects of the diatom *Cyclotella cryptica* (*Bacillariophyceae*): Effect of some environmental factors. *J. Biosci. Bioeng.* **2010**, *109*, 235–239. [CrossRef] [PubMed]
44. Rogato, A.; De Tommasi, E. Physical, Chemical, and Genetic Techniques for Diatom Frustule Modification: Applications in Nanotechnology. *Appl. Sci.* **2020**, *10*, 8738. [CrossRef]
45. Xu, Y.; Zhang, X.; Liu, X.; Wang, G. Alterations of physical properties and microstructure of marine diatomite owing to variation of diatom content. *Mar. Georesour. Geotechnol.* **2022**, *41*, 376–387. [CrossRef]
46. Ruge, J.; Castro, W.; Camacho, J.; Molina, F. Dependencia de las propiedades de retención de agua en suelos caoliníticos con contenidos de microalgas fosilizadas adicionadas artificialmente. In *Geotechnical Engineering in the XXI Century: Lessons Learned and Future Challenges*; IOP Press: Bristol, UK, 2019; pp. 780–787. Available online: https://ebooks.iospress.nl/publication/53323 (accessed on 1 December 2024).
47. Hong, Z.; Tateishi, Y.; Han, J.; Asce, M. Experimental Study of Macro- and Microbehavior of Natural Diatomite. *J. Geotech. Geoenviron. Eng.* **2006**, *132*, 603–610. [CrossRef]
48. Crawford, S.A.; Higgins, M.J.; Mulvaney, P.; Wetherbee, R. Nanostructure of the diatom frustule as revealed by atomic force and scanning electron microscopy. *J. Phycol.* **2001**, *37*, 543–554. [CrossRef]
49. Caicedo, B.; Mendoza, C.; López, F.; Lizcano, A. Behavior of diatomaceous soil in lacustrine deposits of Bogotá, Colombia. *J. Rock Mech. Geotech. Eng.* **2018**, *10*, 367–379. [CrossRef]
50. Dobrosielska, M.; Dobrucka, R.; Gloc, M.; Brząkalski, D.; Szymański, M.; Kurzydłowski, K.J.; Przekop, R.E. A new method of diatomaceous earth fractionation—A bio-raw material source for epoxy-based composites. *Materials* **2021**, *14*, 1663. [CrossRef] [PubMed]
51. Karp-Boss, L.; Gueta, R.; Rousso, I. Judging Diatoms by Their Cover: Variability in Local Elasticity of Lithodesmium undulatum Undergoing Cell Division. *PLoS ONE* **2014**, *9*, e109089. [CrossRef] [PubMed]
52. Gebeshuber, I.; Kindt, J.; Thompson, J.; Del Amo, Y.; Stachelberger, H.; Brzezinski, M.; Stucky, G.; Morse, D.; Hansma, P. Atomic force microscopy study of living diatoms in ambient conditions. *J. Microsc.* **2003**, *212*, 292–299. [CrossRef] [PubMed]
53. Higgins, M.; Crawford, S.; Mulvaney, P.; Wetherbee, R. Characterization of the Adhesive Mucilages Secreted by Live Diatom Cells using Atomic Force Microscopy. *Protist* **2002**, *153*, 25–38. [CrossRef]
54. Losic, D.; Short, K.; Mitchell, J.; Lal, R.; Voelckler, N. AFM Nanoindentations of Diatom Biosilica Surfaces. *Langmuir* **2007**, *23*, 5014–5021. [CrossRef]
55. Diaz, M.; Ma, K.; Schoenung, J.; Dávila, P. An integrated approach for probing the structure and mechanical properties of diatoms: Toward engineered nanotemplates. *Acta Biomater.* **2015**, *25*, 313–324. [CrossRef]
56. Young, A.; Karp-Boss, L.; Jumars, P.; Landis, E. Quantifying diatom aspirations: Mechanical properties of chain-forming specie. *Limnol. Oceanogr.* **2012**, *57*, 1789–1801. [CrossRef]
57. Francius, G.; Tesson, B.; Dague, E.; Dufren, Y.; Martin, V. Nanostructure and nanomechanics of live Phaeodactylum tricornutum morphotypes. *Environ. Microbiol.* **2008**, *10*, 134–1356. [CrossRef]
58. Pletikapić, G.; Berqueand, A.; Misic, T.; Svetlicic, V. Quantitative Nanomechanical Mapping of Marine Diatom in Seawater Using Peak Force Tapping Atomic Force Microscopy. *J. Phycol.* **2012**, *48*, 174–185. [CrossRef]
59. Yao, S.; Subhash, G.; Maiti, S. Analysis of Nanoindentation Response of Diatom Frustules. *J. Nanosci. Nanotechnol.* **2007**, *7*, 4465–4472. [CrossRef]
60. Zgłobicka, I.; Krzysztof, J. Multi-length scale characterization of frustule showing highly hierarchal structure in the context of understanding their mechanical properties. *Mater. Today Commun.* **2022**, *33*, 104741. [CrossRef]
61. Korayem, M.H.; Khaksar, H. Investigating the impact models for nanoparticles manipulation based on atomic force microscope (according to contact mechanics). *Powder Technol.* **2019**, *344*, 17–26. [CrossRef]
62. Kontomaris, S.V.; Malamou, A.; Stylianou, A. The Hertzian theory in AFM nanoindentation experiments regarding biological samples: Overcoming limitations in data processing. *Micron* **2022**, *155*, 103228. [CrossRef]
63. Kontomaris, S.-V. The Hertz Model in AFM Nanoindentation Experiments: Applications in Biological Samples and Biomaterials. *Micro Nanosyst.* **2018**, *10*, 11–22. [CrossRef]
64. JPK Instruments Determining the Elastic Modulus of Biological Samples Using Atomic Force Microscopy. 2022. Available online: https://www.jpk.com/app-technotes-img/AFM/pdf/jpk-app-elastic-modulus.14-1.pdf (accessed on 16 May 2022).
65. Kontomaris, S.V.; Georgakopoulos, A.; Malamou, A.; Stylianou, A. The average Young's modulus as a physical quantity for describing the depth-dependent mechanical properties of cells. *Mech. Mater.* **2021**, *158*, 103846. [CrossRef]

Disclaimer/Publisher's Note: The statements, opinions and data contained in all publications are solely those of the individual author(s) and contributor(s) and not of MDPI and/or the editor(s). MDPI and/or the editor(s) disclaim responsibility for any injury to people or property resulting from any ideas, methods, instructions or products referred to in the content.